

Article

Polymeric Nanoparticles with Embedded Eu(III) Complexes as Molecular Probes for Temperature Sensing

Kirill M. Kuznetsov ¹, Vadim A. Baigildin ¹, Anastasia I. Solomatina ¹ , Ekaterina E. Galenko ², Alexander F. Khlebnikov ² , Victor V. Sokolov ², Sergey P. Tunik ^{1,*} and Julia R. Shakirova ^{1,*}

¹ Department of General and Inorganic Chemistry, Institute of Chemistry, St. Petersburg State University, St. Petersburg 198504, Russia

² Department of Organic Chemistry, Institute of Chemistry, St. Petersburg State University, St. Petersburg 198504, Russia

* Correspondence: sergey.tunik@spbu.ru (S.P.T.); y.r.shakirova@spbu.ru (J.R.S.)

Abstract: Three novel luminescent Eu(III) complexes, **Eu1–Eu3**, have been synthesized and characterized with CHN analysis, mass-spectrometry and ¹H NMR spectroscopy. The complexes display strong emission in dichloromethane solution upon excitation at 405 and 800 nm with a quantum yield from 18.3 to 31.6%, excited-state lifetimes in the range of 243–1016 ms at 20 °C, and lifetime temperature sensitivity of 0.9%/K (**Eu1**), 1.9%/K (**Eu2**), and 1.7%/K (**Eu3**). The chromophores were embedded into biocompatible latex nanoparticles (**NPs_Eu1–NPs_Eu3**) that prevented emission quenching and kept the photophysical characteristics of emitters unchanged with the highest temperature sensitivity of 1.3%/K (**NPs_Eu2**). For this probe cytotoxicity, internalization dynamics and localization in CHO-K1 cells were studied together with lifetime vs. temperature calibration in aqueous solution, phosphate buffer, and in a mixture of growth media and fetal bovine serum. The obtained data were then averaged to give the calibration curve, which was further used for temperature estimation in biological samples. The probe was stable in physiological media and displayed good reproducibility in cycling experiments between 20 and 40 °C. PLIM experiments with thermostated CHO-K1 cells incubated with **NPs_Eu2** indicated that the probe could be used for temperature estimation in cells including the assessment of temperature variations upon chemical shock (sample treatment with mitochondrial uncoupling reagent).

Keywords: luminescent europium complexes; lifetime temperature sensitivity; latex nanospecies; phosphorescence lifetime imaging; intracellular localization; cell thermometry



Citation: Kuznetsov, K.M.; Baigildin, V.A.; Solomatina, A.I.; Galenko, E.E.; Khlebnikov, A.F.; Sokolov, V.V.; Tunik, S.P.; Shakirova, J.R. Polymeric Nanoparticles with Embedded Eu(III) Complexes as Molecular Probes for Temperature Sensing. *Molecules* **2022**, *27*, 8813. <https://doi.org/10.3390/molecules27248813>

Academic Editors: You-Xuan Zheng and Shaojun Yuan

Received: 10 November 2022

Accepted: 6 December 2022

Published: 12 December 2022

Publisher's Note: MDPI stays neutral with regard to jurisdictional claims in published maps and institutional affiliations.



Copyright: © 2022 by the authors. Licensee MDPI, Basel, Switzerland. This article is an open access article distributed under the terms and conditions of the Creative Commons Attribution (CC BY) license (<https://creativecommons.org/licenses/by/4.0/>).

1. Introduction

The growing interest in noninvasive thermometry with high spatial and temporal resolution is largely due to the importance of these kind of measurements for understanding critical features of physiological processes at the cellular level [1–3]. Among various techniques used in this area, luminescent microscopy based on different thermosensitive probes is one of the most reliable and convenient methods because of the fast and reversible response to temperature changes and high spatial resolution up to a few hundred nanometers [4–6]. Small-molecule luminescent probes suitable for nanothermometry can be divided into three major classes [7] depending on the key characteristics of their emission: fluorescent [8,9] and phosphorescent [10,11] thermosensitive chromophores with excited-state lifetime in the nanosecond and microsecond domains, respectively, and lanthanide compounds [7,12–15], which display lifetimes in the range from several hundred μ s to 2 ms. These types of probes are now widely used for temperature measurements in bio-samples of different nature (see reviews [1,5,6,16] and some recent research papers [17–19]). However, the application of these probes in biomedical studies faces some problems characteristic of the certain types of emitters that are a consequence of the specific features

of their photophysical properties. Fluorescent compounds constitute the largest group of thermosensors potentially applicable in biological studies [8], which suffer from low bleaching stability and the biasing effect of the sample background emission interfering with the probe signal both in ratiometric and lifetime-based modalities [20]. In addition, the dynamic interval of a probe fluorescence lifetime is limited to several nanoseconds, which complicates the measurements in the lifetime domain technically and makes the corresponding equipment rather expensive [20]. The phosphorescent thermosensitive transition metal complexes of Ru(II) [21,22], Ir(III) [23], and Pt(II) [24,25] are largely free from the disadvantages of the fluorescent emitters mentioned above but they naturally display a strong effect of oxygen quenching onto their emission parameters that results in the crosstalk between two environmental characteristics (e.g., T-O₂), which may considerably distort the results of temperature sensing. The thermosensors based on lanthanide complexes [7,20,26–28] display a large Stokes shift and a wide dynamic interval of lifetimes, show no emission quenching with molecular oxygen, and demonstrate high emission and lifetime response to temperature variations in physiologically relevant intervals, of which Eu(III) organometallic compounds [29] are the most promising candidates for temperature measurements. Nevertheless, the most significant disadvantage of this type of sensor for bioimaging applications is extremely strong emission quenching in aqueous media. The quenching mechanism consists of vibrational energy transfer to water molecules [30]; therefore, the isolation of these chromophores from interaction with the solvent by embedding into water-impermeable polymeric nanospecies is an approach of choice in the design of effective europium temperature sensors.

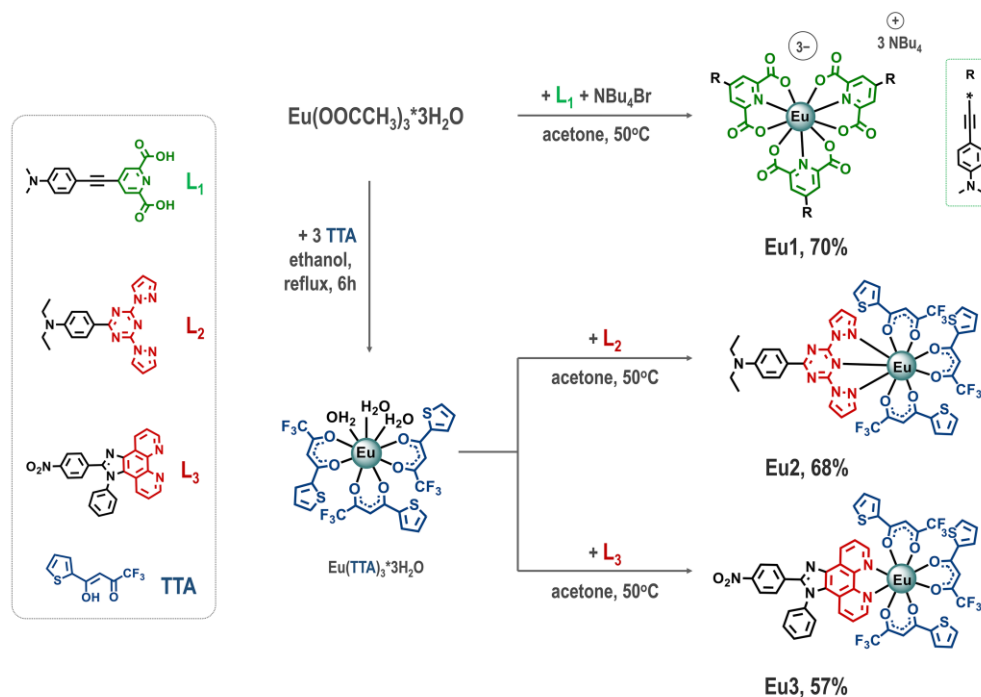
In our previous study [31], we used nanoemulsion polymerization to incorporate thermosensitive Eu(III) complexes into latex nanoparticles (NPs) that effectively prevented europium emission quenching. The obtained NPs displayed a rather high lifetime response to temperature variations (a sensitivity up to 0.84%/K and resolutions of 0.26 K) and complete reversibility in cycling experiments that made them promising for application in biomedical studies. However, the emission of these europium chromophores can be excited only with UV irradiation at 365 nm which is far beyond the biologically friendly interval, and the chemical composition of the NPs does not imply their vectorization for the targeted delivery of the sensor to a certain cell compartment or tissue. In the present study, we applied the other europium complexes, which allowed emission generation upon excitation either in the visible range of spectrum (405 nm) or with two-photon excitation (800 nm) that made the nanothermometers applicable in prolonged biological experiments without damage to the samples under study. The photophysical properties of the obtained NPs were studied in detail along with investigation of their lifetime sensitivity to temperature in different media. We also modified the polymerization technique by using 2-aminoethyl methacrylate as a component of the polymerization reaction that results in the NPs' surface amination and opens the way to the NPs' vectorization, e.g., with a phosphonium cation. The suitability of the NPs for temperature mapping in cells using phosphorescent lifetime measurements (PLIM) was tested in CHO-K1 cell culture.

2. Results and Discussion

2.1. Synthesis of Thermosensitive Eu(III) Complexes

In this study, the choice of the ligands in the Eu(III) ion environment was dictated by the necessity to shift the excitation wavelength of the final complexes into a biologically friendly interval, at least to the wavelengths >400 nm, that would make it possible to use a "blue" 405 nm laser, which is a standard component of luminescent microscopy equipment. To meet this requirement, we introduced into the coordination sphere of europium complexes the ligands (L₁L₃, Scheme 1) containing developed aromatic systems that, as a rule, results in a bathochromic shift of the absorption/excitation wavelength. Indeed, absorption and excitation spectra of L₁–L₃ are extended well below 400 nm (see Figure S9), thus giving a chance to generate emission of the corresponding europium complexes with the 405 nm laser. These ligands also contain spatially separated donor/acceptor diads that make them

promising from the viewpoint of two-photon absorption and the possibility to be excited by using near-infrared irradiation at about 800 nm. This type of low-energy excitation is even more promising for the microscopic studies of biological samples. **L**₁ [32,33] and **L**₂ [34] were obtained according to the published procedures; **L**₃ is a novel diimine ligand based on the imidazophenanthroline aromatic system with an electron-withdrawing NO₂ group in a phenyl substituent. The synthesis and characterization of **L**₃ is described in the experimental section; its synthetic scheme, proton NMR, and ESI⁺ mass-spectra are given in Electronic Supporting Information (ESI)—see Scheme S1 and Figures S1 and S5.



Scheme 1. Synthesis of europium complexes.

Eu1, **Eu2**, and **Eu3** complexes were synthesized using the standard procedures for the preparation of europium tris-chelates [28] and $[\text{Eu}(\text{TTA})(\text{diimine})]$ [34] emitters; see Scheme 1. The target compounds were obtained in a good yield, and purified and characterized using elemental analysis, HR ESI⁺ mass-spectrometry (Figures S5–S8), and ¹H NMR spectroscopy (Figures S2–S4). The positions of the signals in mass spectra and their isotopic distributions were in excellent agreement with the suggested stoichiometry of the obtained compounds. The ¹H NMR spectra displayed a low-field shift of the corresponding proton signals typical for Eu(III) complexes; the number of signals and their relative intensity and multiplicity fit well with the structural patterns shown in Scheme 1 and allowed the complete assignment of the resonances observed (Figures S1–S4).

2.2. Photophysical Properties of Eu(III) Complexes

The obtained **Eu1–Eu3** complexes luminesce in dichloromethane solution; their absorption, excitation, and emission spectra are shown in Figure 1 and Figures S10–S12, and the major photophysical characteristics are summarized in Table 1.

In dichloromethane (DCM) solution, all complexes displayed emission bands typical for Eu(III)-based chromophores with the major component located at 612 nm. The emission of **Eu1** and **Eu2** may be excited with a 405 nm laser that makes possible their use in imaging experiments without photodamage to the sample under study. Moreover, both complexes showed appreciable two-photon absorption under excitation at 800 nm, thus increasing their suitability for bioimaging experiments. **Eu2** also displayed independent fluorescence of coordinated **L**₂ (Figure 1) that, in principle, provides an opportunity for ratiometric measurements. On the contrary, **Eu3** gave appreciable emission intensity only by using the

ultraviolet 365 nm laser radiation that considerably limits its application in the studies of biological objects. In DCM, the complexes displayed rather high emission quantum yields ranging from 18.3 to 31.6% and lifetimes in the interval from two hundred μs to one ms (Table 1). The lifetimes of **Eu1–Eu3** demonstrated a substantial temperature dependence in the physiologically relevant interval (see Figure 1b, Figures S12 and S13) which can be approximated by Equation (S1); see ESI [4,35].

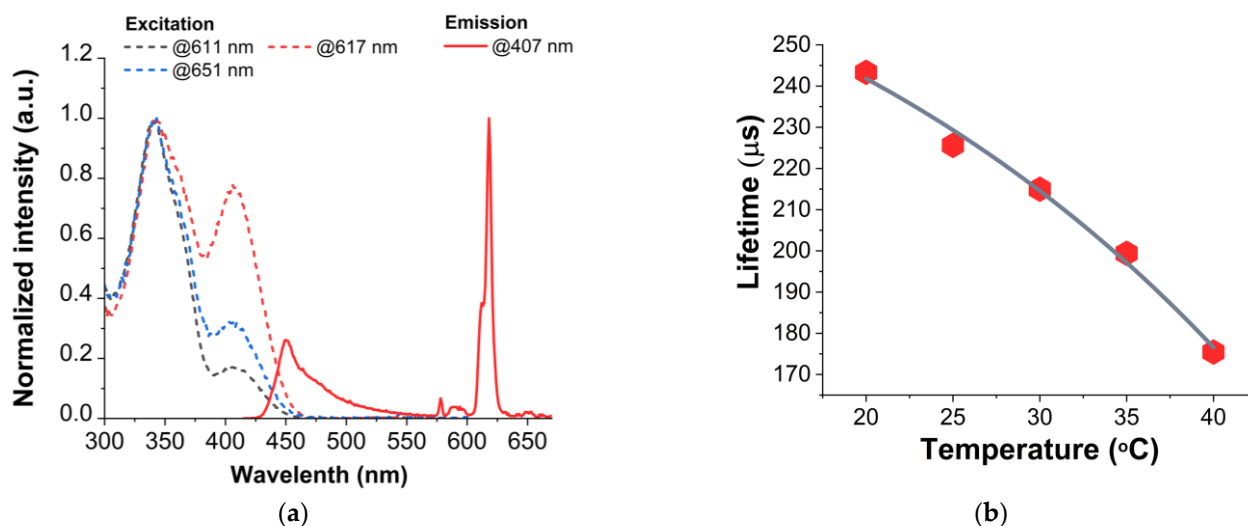


Figure 1. (a) Excitation (dashed lines) and emission (solid line) spectra of **Eu2**, 293 K; (b) lifetime temperature dependence of **Eu2** in dichloromethane; the interpolation of experimental data was performed using Equation (S1).

Table 1. Summary of Photophysical Properties of Eu(III) Complexes and NPs.

Sample	λ_{abs} , nm	λ_{exc} , nm	Φ , % ³	$\tau_{20^\circ\text{C}}/\tau_{40^\circ\text{C}}$, μs	S_r , %/K	σ_{TPE} , GM
Eu1 ¹	275, 383	384	18.3 \pm 1.4	1016/857	0.9	133
Eu2 ¹	344, 391	340, 407	25.2 \pm 1.4	243/176	1.9	87
Eu3 ¹	274, 368	341, 360	31.6 \pm 2.7	622/463	1.7	44
NPs_Eu1 ²	-	374	10.2 \pm 0.1	1017/877	0.8	-
NPs_Eu2 ²	-	338, 405	16.3 \pm 0.1	538/430	1.3	-
NPs_Eu2_TPP ²	-	292, 348	16.8 \pm 0.1	555/478	0.8	-
NPs_Eu3 ²	-	340, 358	17.0 \pm 0.1	685/604	0.7	-

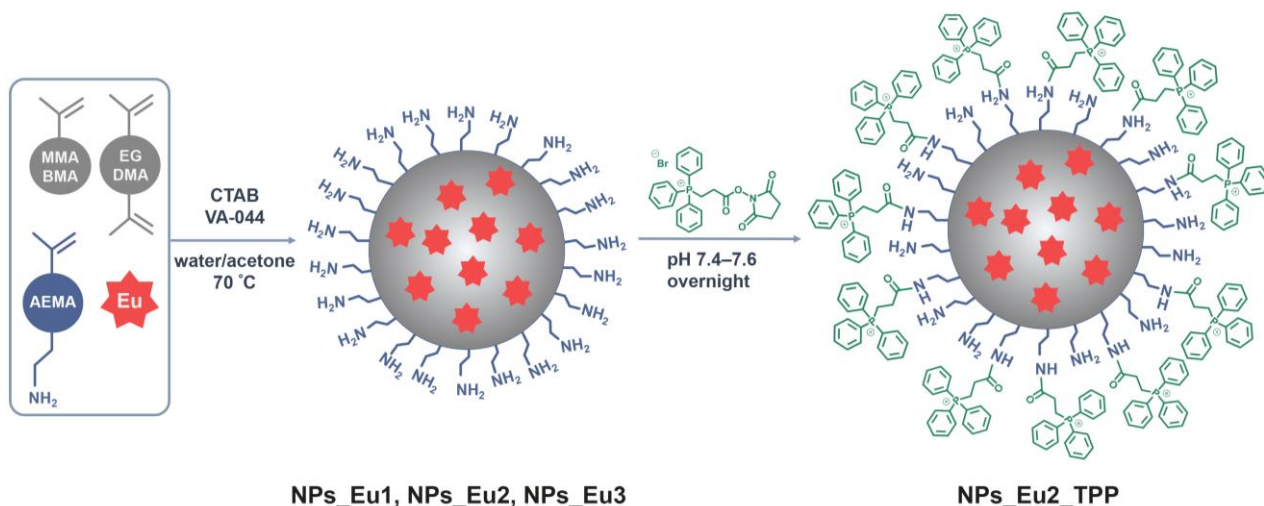
¹ in dichloromethane solution, ² in aqueous dispersion, ³ λ_{ex} 365 nm; λ_{abs} —absorption wavelengths, λ_{exc} —excitation wavelengths measured at the 612 nm emission band, Φ —quantum yield, $\tau_{20^\circ\text{C}}$ and $\tau_{40^\circ\text{C}}$ —excited-state lifetimes at 20 and 40 °C, respectively, S_r —relative temperature sensitivity, σ_{TPE} —two-photon absorption cross-section measured using 800 nm excitation.

These experimental data also allow calculating the emitters' temperature sensitivity (S_T , Equation (S3)) and relative temperature sensitivity (S_r , Equation (S4)); the latter showed the highest value of 1.9%/K for **Eu2** that makes the complexes promising for application in nanothermometry. To avoid europium emission quenching in the aqueous/physiological media, we used an approach successfully applied in our previous study [31], namely, the incorporation of these emitters into latex nanoparticles.

2.3. Synthesis of Latex Nanoparticles (NPs)

The first generation of thermosensitive NPs described in our previous publication [31] demonstrated that europium complexes' incorporation into latex nanoparticles prevents emission quenching in aqueous media and also makes their emission characteristics completely reversible in thermocycling experiments at least during nine cycles. The NP positive

charge brought on by the surfactant, cetyltrimethylammonium bromide (CTAB), essentially facilitates adsorption onto cell membranes and subsequent probe internalization [36]; however, the absence of surface functional groups suitable for conjugation with vectors makes the probe uptake non-targetable, giving a random probe distribution in cells that significantly limits their application in bioimaging. Therefore, we prepared the second generation of luminescent NPs (NPs_Eu1–NPs_Eu3) through the introduction of primary amino groups onto the NPs' surface via the use of 2-aminoethyl methacrylate (AEMA) in the polymerization protocol (Scheme 2).



Scheme 2. Synthesis of Eu-containing nanoparticles and their further modification by a triphenylphosphonium cation (MMA—methyl methacrylate, BMA—butyl methacrylate, EG DMA—ethyleneglycol dimethacrylate, AEMA-2—aminoethyl methacrylate, Eu—europium(III) complex).

The numerical photophysical and physicochemical data for NPs_Eu1–NPs_Eu3 are given in Tables 1 and 2, respectively; the absorption, excitation, and emission spectra are shown in Figures S22–S25. The excitation and emission band profiles of the europium-containing nanospecies in aqueous dispersions were essentially similar to those obtained for the parent europium complexes in a DCM solution. However, the emission quantum yields for all NPs displayed a ca. 40% reduction compared to the corresponding complexes in DCM, that may be due to partial emission quenching by solvent molecules or is related to excitation energy transfer to the polymeric matrix. Nevertheless, the emission intensity was still rather high, particularly taking into account the aqueous environment of the chromophores. It is also worth noting that the lifetime sensitivity of the NP probes was reduced to a different extent depending on the nature of the europium emitter; the strongest decrease was observed in the case of NPs_Eu3, whereas NPs_Eu2 displayed an appreciable S_r magnitude equal to 1.3%/K, still the highest in this group of nanosensors.

Table 2. Summary of physicochemical characteristics of phosphorescent NPs.

Sample	Size, nm				ζ -Potential, mV	NH ₂ -Groups, $\mu\text{mol}/\text{m}^2$	Number of Eu Complex per Particles	Number of TPP per Particles
	DLS	PDI	TEM ¹	TEM ²				
NPs_Eu1	116	0.07	85	76	40.0	0.74	350	- ³
NPs_Eu2	100	0.06	76	67	31.6	0.84	800	- ³
NPs_Eu2_TPP	99	0.11	76	67	24.0	0.07	800	22,800
NPs_Eu3	101	0.14	79	69	22.4	0.82	425	- ³

¹ TEM pictures with negative staining by UrAc; ² TEM pictures without negative staining; ³ not determined as NPs were not used for modification by triphenylphosphine.

The diameter of the NPs_Eu1 was found to be 116 nm with a PDI of 0.07 (Table 2; Figure S18) as measured using DLS, whereas the average diameter determined using

transmission electron microscopy (TEM) with the negative staining was 85 nm (Table 2, Figure 2a). The latex NPs containing **Eu2** and **Eu3** showed essentially similar size characteristics: the NPs' size equaled ca. 100 nm and had a PDI of 0.07 and 0.14, respectively (Table 2; Figures S19 and S20). A similar decrease in the particle diameter was observed using TEM: the size reduced to 72 and 70 nm for **NPs_Eu2** and **NPs_Eu3**, respectively (Table 2; Figure 2b,c). The difference between the DLS and microscopic measurements is related to the formation of a hydrate shell around the particles in the aqueous dispersions and its shrinking in a dry state [37].

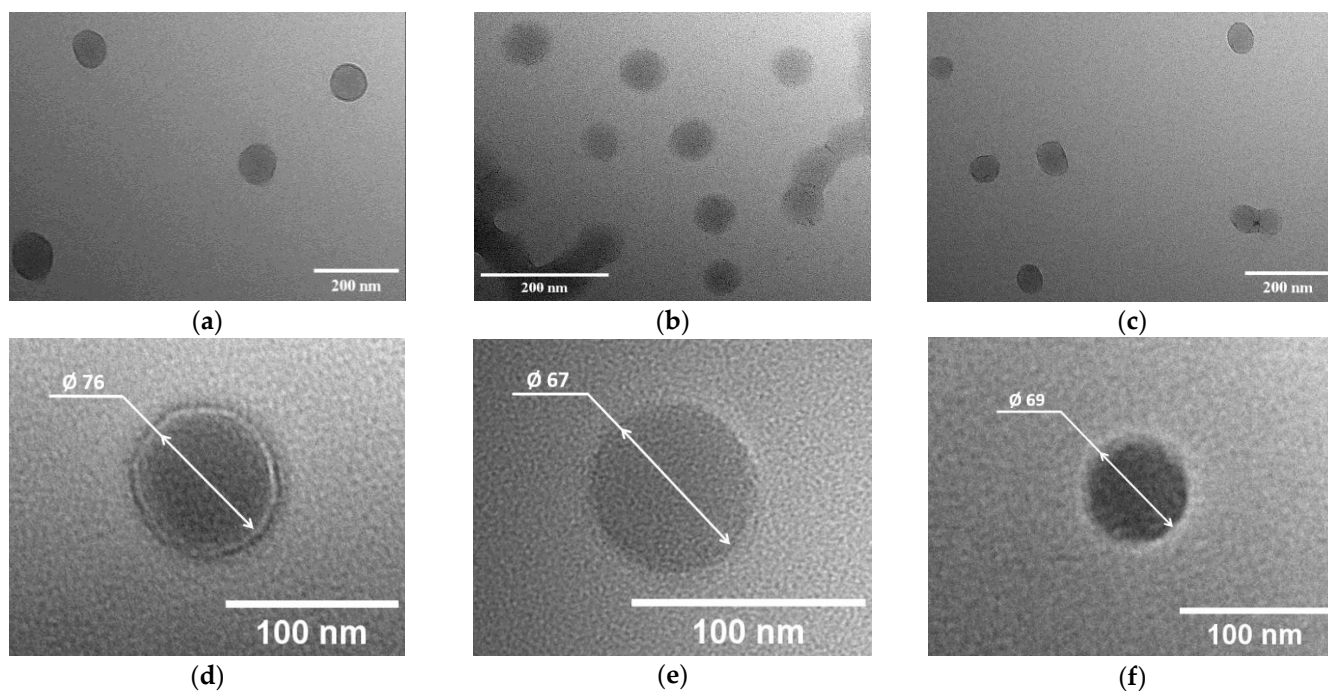


Figure 2. TEM pictures of obtained NPs with incorporated Eu complexes with negative staining by UrAc: (a) **NPs_Eu1**; (b) **NPs_Eu2**; (c) **NPs_Eu3**; without negative staining: (d) **NPs_Eu1**; (e) **NPs_Eu2**; (f) **NPs_Eu3**.

All NPs possessed positive ζ -potentials due to the presence of positively charged quaternary and primary amino groups from CTAB and AEMA, respectively, and imidazoline functions of the VA-044 initiator on the surface. In particular, the ζ -potential of **NPs_Eu1** equaled 40 mV, 31.6 mV for **NPs_Eu2**, and reached only 22.4 mV for **NPs_Eu3** (Table 2; Figures S18–S20). The magnitude of the ζ -potential and wider size distribution of **NPs_Eu3** compared to **NPs_Eu1** and **NPs_Eu2** evidence a weak colloid stability of the former that can lead to the aggregation in the presence of biological molecules or upon an increase in media salinity. These observations, together with the necessity of the **Eu3** excitation with UV laser radiation and the lowest S_r value, indicate that its applicability is severely limited in the studies of biological objects.

The next step in the NPs' structure investigation was the estimation of the complexes' location within the nanoparticles. To understand how deep the Eu emitters were localized inside of the NPs, we carried out TEM without negative staining that allows detecting the heavy elements such as europium. The size of the NPs obtained from the TEM pictures is shown in Figure 2d–f and Table 2. All NPs demonstrated a size smaller than that observed in the experiments with negative staining by uranyl acetate (UrAc): the decrease in NPs' diameters equaled 9–10 nm. A comparison of the results obtained with and without negative staining indicates that emitter molecules were localized in the NPs under the ca. 5nm-thick surface layer. Therefore, the outer layer containing a cross-linked polymer structure blocked the water permeability into the core which prevented luminescence

quenching for at least 1.5 years that we observed during the development of the sensor. These data are in a good agreement with those presented in our previous article, where X-ray photoelectron spectroscopy was used to demonstrate the absence of europium in the surface layer [31].

We also calculated the number of complexes per particle using the data on the NPs' size and their composition determined by ICPOES (Table 2, Equation (S2) in ESI) that gave the average value from 350 to 800 molecules of Eu complexes per particle. Interestingly, the number of the complex molecules in **NPs_Eu2** was ca. two times higher than the magnitudes obtained for the other species. The reason for this difference is not clear and requires the investigation of the polymerization mechanism in more detail. However, the higher amount of **Eu2** per particle can be favorable for biological experiments as it increases the brightness of phosphorescence, decreases the amount of NPs needed for each experiment, and reduces the signal accumulation time.

To finally choose the most promising candidate for biological studies, we estimated the NPs' lifetime sensitivity in a physiological temperature range from 20 to 40 °C. **NPs_Eu1** and **NPs_Eu2** were only used in these experiments as the application of **NPs_Eu3** in biological studies is limited due to the necessity of excitation with UV laser radiation and low colloid stability as mentioned above. The dependence of lifetime on temperature for **NPs_Eu1** and **NPs_Eu2** is presented in Figures S26 and S27. The lifetime of **NPs_Eu1** varied in the range 1020–870 μ s, whereas the lifetime of **NPs_Eu2** changed from 520 to 430 μ s at 20 and 40 °C, respectively, which points to a substantially shorter time for the data acquisition in PLIM experiments in the latter case. The whole set of data obtained for the **NPs_Eu2** particles—highest temperature sensitivity, emission excitation with visible light, high colloidal stability, and shortest lifetime among the studied NPs—indicates that the **NPs_Eu2** is the most promising probe for spatial and temporal temperature monitoring in biological systems by using the PLIM modality. These considerations prompted us to study in detail the dependence of the **NPs_Eu2** probe lifetime on the temperature between 20 and 40 °C in water, Dulbecco's phosphate buffer (DPB), and in the model physiological media (Dulbecco's modified eagle medium (DMEM) supplemented with 10% fetal bovine serum (FBS)), which simulates the microenvironment of the probe in biological samples to a maximum extent; see Figure 3.

The data given in Figure 3a show that the calibration curve built up for the water solution differed substantially to those obtained in DPB and the DMEM + 10% FBS mixture, whereas the data for the two latter media are very close each other. The difference in the probe behavior observed for water and solutions with substantial salinity looks systematic and can be explained by the electrostatic interaction of the NPs with cations that may change the emitter lifetime response to variations in the media temperature. However, this difference falls in the limits of experimental uncertainty (ca. 5%) that make it possible to use all three sets of data for the calibration of lifetime vs. temperature dependence. Additionally, we checked the effect of the other environment stimuli (pH and viscosity; see Figure 3a) that showed a lifetime independence on these media characteristics. Thus, all obtained data have been used to build up a general calibration curve shown in Figure 3b which gave the relative temperature sensitivity of the sensor 1.3%/K. In the last decade, several lifetime-based temperature sensors have been obtained and applied for in vitro and in vivo biological experiments; see data in Table S2 [31,38–46]. Two of them displayed a strong temperature sensitivity of ca. 7.5%/K [38] and 6.3%/K [39] but they were not without rather serious drawbacks. The nanocapsule sensor, based on excitation energy transfer from a palladium phthalocyanine photosensitizer onto a perylene emitter [38] through a chemical reaction, displayed an extremely long lifetime (second range!), which was eventually determined by the reaction rate constant. These photophysical characteristics suit in vivo temperature measurements well but cannot be applied for cell experiments in PLIM mode because of the unacceptably long image acquisition. The other effective temperature-sensitive probe (HPS/Butter/DSPE-PEG-Biotin nanorods) [39] was prepared by using a relatively simple technology but needed excitation with UV irradiation and

showed a lifetime in the nanosecond domain that required rather expensive equipment for lifetime measurements. The other temperature sensors working in lifetime mode [31,40–46] displayed a sensitivity comparable to or even lower than that obtained for NPs_Eu2. These observations, together with the possibility to use NPs_Eu2 in PLIM mode to acquire the sensor signal, indicate that this probe is promising for application in cell experiments.

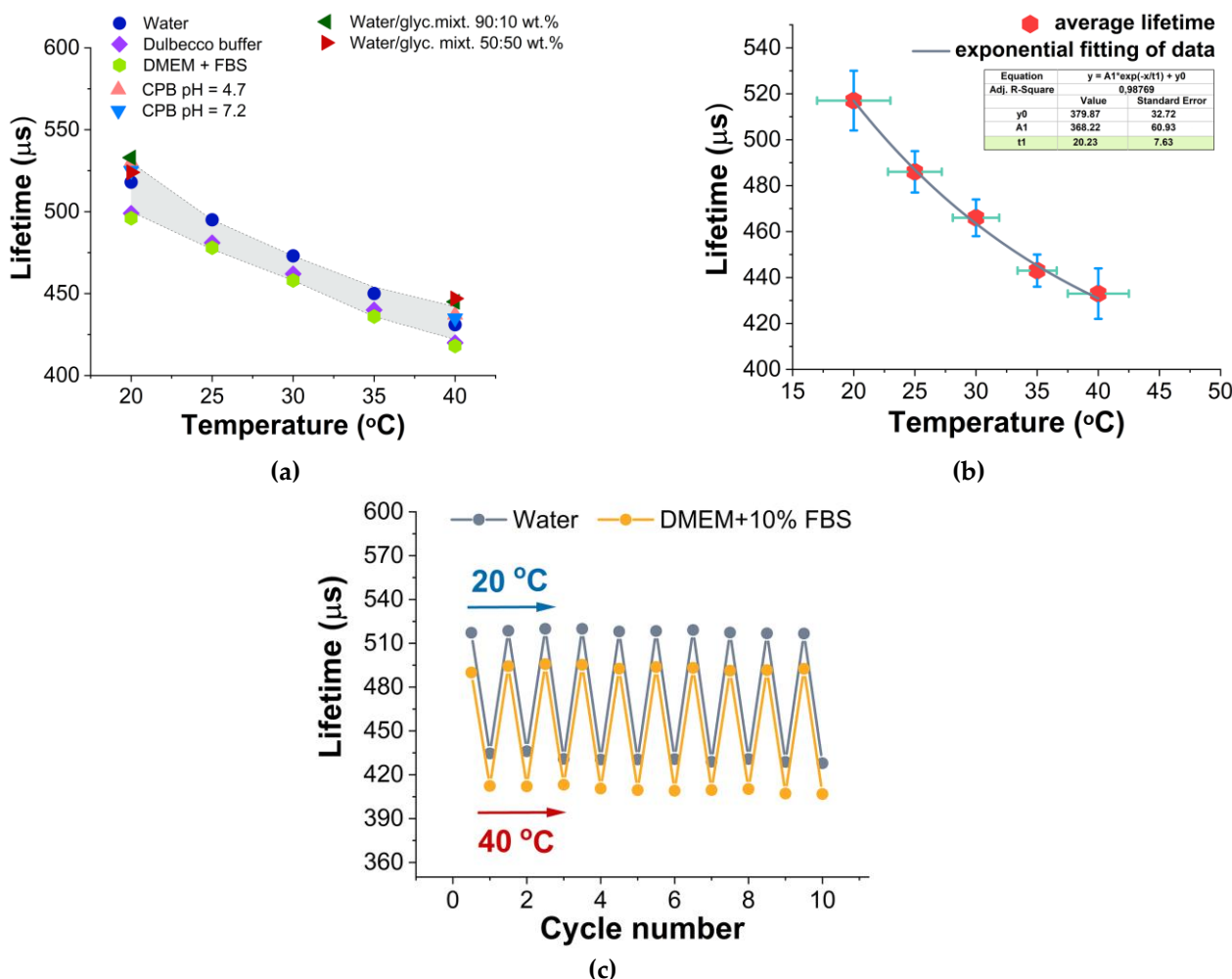


Figure 3. (a) Temperature sensitivity of NPs_Eu2 lifetime in different media: water, Dulbecco’s buffer, and model physiological medium (DMEM + 10% FBS); (b) Calibration curve obtained by using the pool of experimental data given in Table S1 and Figure 3a. Interpolation was performed using Equation (S1); (c) Cyclic lifetime measurements for NPs_Eu2 between 20 and 40 $^{\circ}\text{C}$ in water and DMEM + 10% FBS.

Cyclic temperature measurements between 20 and 40 $^{\circ}\text{C}$ (Figure 3c) were carried out in water dispersion and a DMEM + FBS solution. Similarly to the behavior of the calibration curves described above, these experiments gave different absolute lifetime values for water and DMEM + FBS solutions but displayed very good reproducibility that is of critical importance for temperature monitoring in living objects under different conditions and actions of outer stimuli.

2.4. Cell Experiments

2.4.1. Cytotoxicity and Localization of Probe in Cells

To further assess the applicability of NPs-Eu2 in biological studies, we carried out cytotoxicity tests, and measured the dynamics of the probe uptake and its subcellular distribution in living CHO-K1 cells. The results of the MTT assay are shown in Figure 4a.

The data indicate that the viability of cells was high, up to ca. 10^{-2} wt.% of dry residue. A further increase in the concentration led to a significant increase in the probe toxicity. Therefore, in order to minimize the toxic effect of the probe and maximize the luminescent signal, for subsequent bioimaging experiments, we chose a probe-limiting concentration of 0.0195 wt.% of dry residue or 8.56×10^{-7} mmol in terms of the amount of Eu2 (calculations were performed using Equation (S2); see ESI).

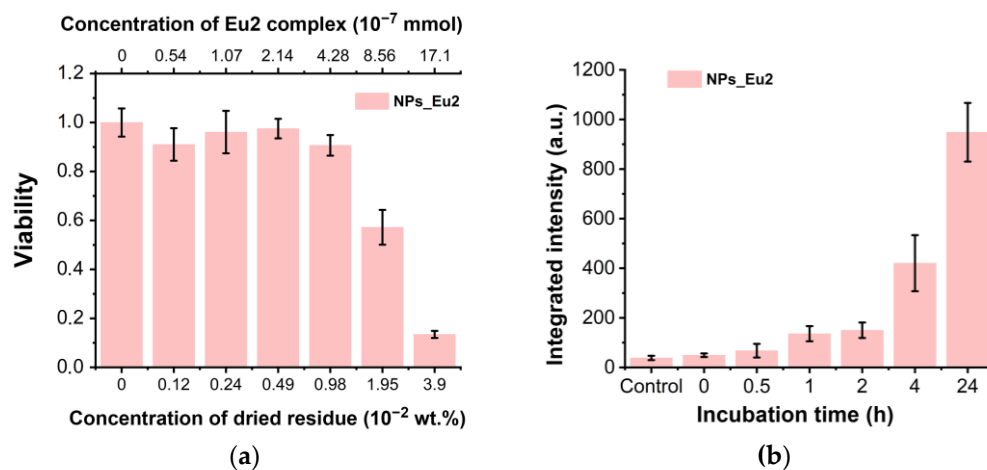


Figure 4. (a) MTT assay of NPs_Eu2 probe; for the definition of NPs' concentration see Experimental Section; (b) The dependence of emission intracellular intensity vs. incubation time of CHO-K1 with NPs_Eu2.

The dynamic of internalization of NPs_Eu2 in living CHO-K1 was monitored using confocal microscopy with excitation at 405 nm in two emission channels: 500–550 nm and 570–620 nm (Figure S29). The emission of the probe could be detected in the cell cytoplasmic region already after 1 h of incubation. The emission intensity, however, grew slowly, reaching a maximum after 24 h of incubation. Based on the results of cytotoxicity and the dynamics of probe uptake, a probe concentration of 0.0195 wt.% and incubation time of 24 h were chosen for further experiments.

To reveal the localization of the probe in cellular compartments, CHO-K1 cells were co-stained with NPs_Eu2 and the commercial dyes LysoTracker Deep Red and BioTracker 405 Blue, which are fluorescent probes for acidic organelles and mitochondria, respectively. Unfortunately, the blue fluorescence of the ligand (see above) overlapped the mitochondria tracker signal which prevented the assessment of the probe accumulation in this cellular compartment. Nevertheless, confocal microscopy of CHO-K1 cells co-stained with NPs_Eu2 and LysoTracker Deep Red (Figure 5) showed that the probe was predominantly localized in acidified cell compartments (endosomes of different types and lysosomes) that most probably indicates the probe uptake by endocytic mechanisms or micropinocytosis [47].

2.4.2. PLIM Experiments

As an evaluation of applicability of the nanoparticles obtained for intracellular temperature measurements, a series of PLIM experiments were carried out. In the first one, living CHO-K1 cells stained with NPs_Eu2 were thermostated for 40 min prior to microscopy and during the experiment at 30 °C and 40 °C; Figure 6.

The elevation of temperature by 10 degrees (from 30 to 40 °C) led to a decrease in the probe lifetime by ca. 50 μ s (from 480 to 430 μ s). The maxima of lifetime distribution fit well the calibration curve data obtained in the solution (Figure 3b). It is important to note that the lifetime distribution across the whole image is rather broad with a width at half-height of ca. 25 μ s that can be assigned to the temperature variation in different compartments of the living cells as well as to the accuracy of lifetime measurements (5%, see above). Thus,

the obtained results indicate that the probe can be used for measurements of temperature in the cells.

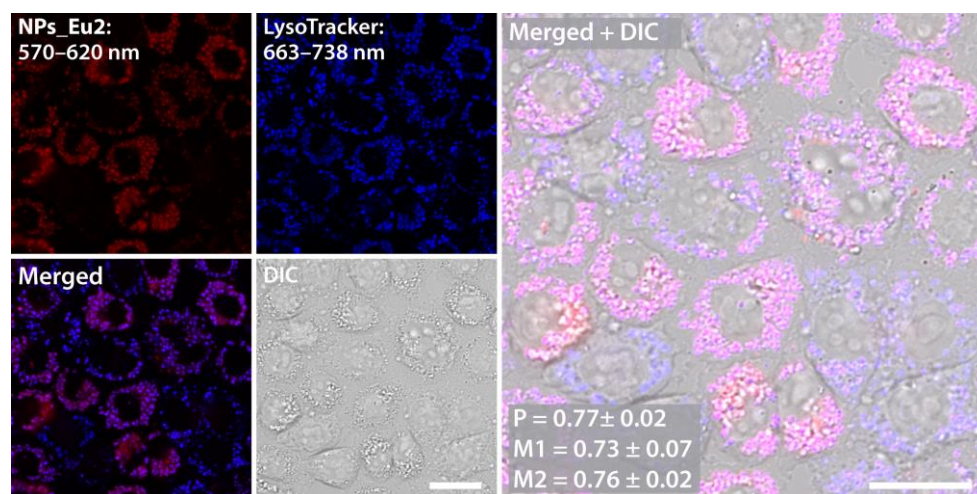


Figure 5. Subcellular distribution of LysoTracker Deep Red (blue color), and NPs_Eu2 (red color) in CHO-K1 cells. Pearson's (P) and Manders' overlap coefficients (M1—fraction of tracker signal that overlaps conjugate signal, M2—fraction of conjugate signal that overlaps tracker signal) are presented as mean \pm standard deviation calculated for 50 cells. Scale bar, 20 μm .

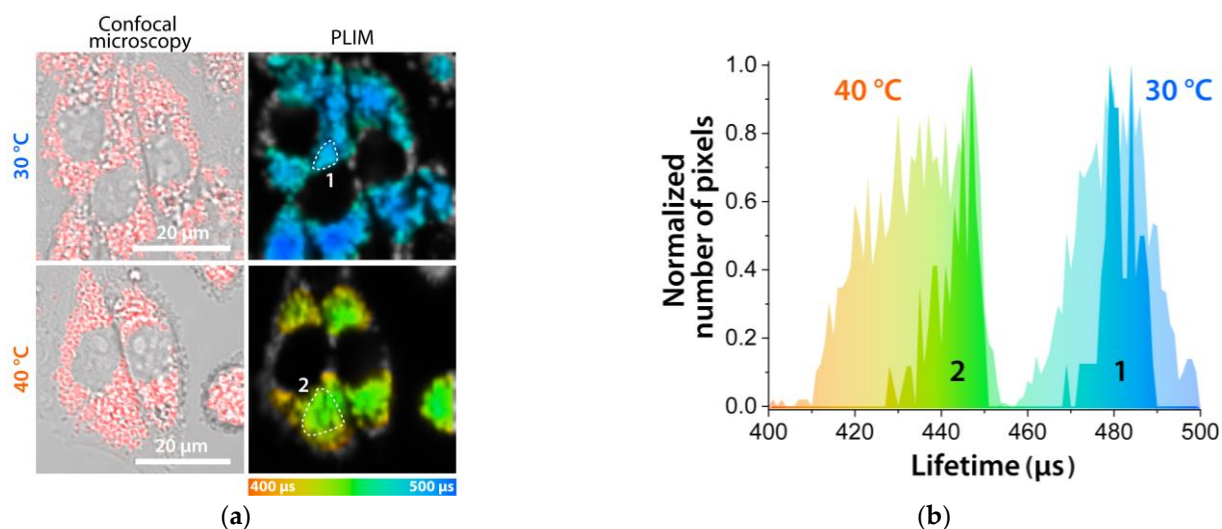


Figure 6. PLIM of CHO-K1 cells incubated with NPs_Eu2 0.0195 wt%, 24 h: (a) Confocal/DIC microscopy (left) and PLIM (right) at two temperatures 30 (up) and 40 (bottom) °C. The colors from red to blue denote lifetimes from 400 to 500 μs . (b) Normalized lifetime distribution of the whole images and selected regions № 1 and 2.

In the second series of PLIM experiments, we monitored the probe lifetime variations as a measure of cell physiological response to the action of chemical *stimuli*, namely, the addition of mitochondrial uncoupling agent (carbonyl cyanide-4-(trifluoromethoxy) phenylhydrazone, FCCP), which usually gives an increase in cell temperature [48–51] due to the inhibition of ATP synthesis in the mitochondria and the induction of energy release in the form of heat [46,52].

Analysis of the lifetime distribution across the studied images, see Figure 7, indicates that the probe lifetime gradually dropped down after the addition of FCCP for ca. 20 μs , indicating an increase in intracellular temperature by ca. 3–4 °C, which is close to the values found in the similar cell experiments [51].

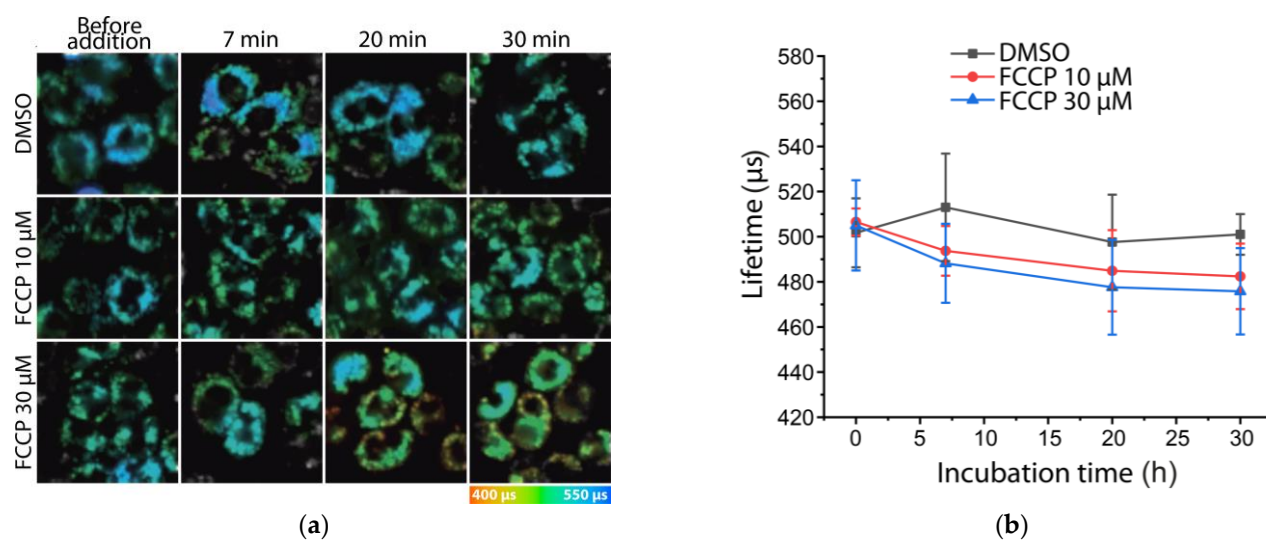


Figure 7. (a) PLIM of CHO-K1 cells incubated with **NPs_Eu2** (0.0195 wt.%, 24 h) at RT (25 °C) and after addition of DMSO and DMSO solution of FCCP (10 μM and 30 μM): A. PLIM images. The color variations from red to blue denote lifetimes from 400 to 550 μs; (b) Dependence of the maximum of lifetime distribution in PLIM images over time. The uncertainty bars denote the half-width of the lifetime distribution across the whole image.

2.5. Modification of Latex NPs' Surface

As mentioned above, modification of the NPs' surface with primary amino groups makes possible the sensor vectorization using a standard chemistry of amide bond formation for the attachment of vector functions to the sensor. To demonstrate the applicability of this approach, we modified the **NPs_Eu2** surface with a phosphonium cation using N-hydroxysuccinimidyl ester of 2-carboxyethyl triphenylphosphonium bromide (**TPP-NHS**); see Scheme 2. The phosphonium cation is a well-known vector for the delivery of molecular objects to the mitochondria, which are the “powerhouse of the cell” [53,54] and may show considerable variations in local temperature [55]. The details of the synthesis and characterization of modified species (**NPs_Eu2_TPP**) are given in the Materials and Methods section and ESI (Figure S30). The successful conjugation of **TPP** was confirmed by the analysis of phosphorus content in the NPs using ICPOES, which showed the presence of **TPP** in the system in the amount of 22,800 molecules per **NPs_Eu2_TPP** particle (Table 2). The obtained NPs displayed a size of 99 nm (measured using DLS, Table 2, Figure S31) which is nearly identical to the magnitude obtained for the **NPs_Eu2** species, but the ζ-potential was decreased to 24 mV (Figure S31) compared to the initial nonmodified species due to a reduction in the number of surface amino groups. It was also found that the photophysical characteristics of the species modified with phosphonium cations were very similar to those of the starting nonmodified **NPs_Eu2** including lifetime sensitivity to temperature variations; see Figures S32 and S33. However, the studies on CHO-K1 cells' incubation with **NPs_Eu2_TPP** showed that this species does not display preferential localization in mitochondria. The experiments on the probe colocalization with LysoTracker Deep Red gave the values of Pearson and Manders coefficients (Figure S34), which are even higher than those obtained for **NPs_Eu2**, which points to the essentially similar behavior of modified and nonmodified probes with respect to mitochondrial accumulation. These observations indicate that, due to so-far unknown reasons, this type of vectorization with phosphonium cations does not give the desired result and it is necessary to search for the other ways of mito-vectors' association with the probes obtained.

3. Materials and Methods

Materials. Methyl methacrylate (98%, MMA) and butyl methacrylate (BMA) were purchased from Acros Organics and distilled under vacuum before use. Ethyleneg-

lycol dimethacrylate (98%, EGDMA, Sigma), 2-aminoethyl methacrylate hydrochloride (AEMA, Sigma), 2,2'-azobis [2-(2-imidazolin-2-yl)-propane]dihydrochloride (97%, VA-044, Sigma), cetyltrimethylammonium bromide (CTAB), and acetone were used as received. Water was purified using a "Simplicity" ("Merck Millipore") water purification system (type 1 water). 1,10-Phenanthroline-5,6-dione [56], Eu(OAc)₃·nH₂O [57], Eu(TTA)₃·3H₂O [58], L1 (4-((4-(dimethylamino)phenyl)ethynyl)pyridine-2,6-dicarboxylic acid [32,33], L2 (4-(4,6-di(1H-pyrazol-1-yl)-1,3,5-triazin-2-yl)-N,N-diethylaniline) [34], and (2-Carboxyethyl)triphenylphosphonium bromide (CE-TTP) [59] were synthesized according to the published procedures. Ligand L3 has not been previously described and its synthesis is presented in this paper. Reagents (Merck KgaA, Darmstadt, Germany), general solvents (Vekton, St. Petersburg, Russia), and deuterated solvents (Carl Roth GmbH + Co. KG, Germany) were used as received without further purification.

General Experimental Details. Mass spectra were recorded using a Bruker maXis HRMS-ESI-QTOF, ESI⁺ or ESI⁻ mode. ¹H and ¹H–¹H COSY (400 MHz) NMR spectra were recorded on a Bruker 400 MHz Avance. Chemical shift values are reported relative to TMS (δ = 0.00). ¹H NMR spectra were referenced to the residual signal of CDCl₃ (7.26 ppm), Acetone-d₆ (2.05 ppm), or DMSO-d₆ (2.50 ppm). Microanalyses were carried out by using Euro EA3028-HT.

Synthesis of L3, 2-(4-nitrophenyl)-1-phenyl-1H-imidazo [4,5-f][1,10]phenanthroline.

According to the previously published procedure (<https://doi.org/10.1002/ejic.202100189>), 4-nitrobenzaldehyde (181 mg, 1.2 mmol, 1 eq.), 1,10-phenanthroline-5,6-dione (252 mg, 1.2 mmol, 1 eq.), aniline (223 mg, 2.4 mmol, 2.5 eq.), and ammonium acetate (185 mg, 2.4 mmol, 2.5 eq.) were added to 7 mL of acetic acid and refluxed overnight. The precipitated powder was centrifuged and washed with diethyl ether to give a yellow powder, which was then recrystallized through gas-phase diffusion of diethyl ether into dichloromethane solution of the product; yield 62%. ¹H NMR (400 MHz, CDCl₃, 297 K) δ = 9.24 (dd, ³J_{H-H} = 4.4, ⁴J_{H-H} = 1.8 Hz, 1H, phen), 9.14 (d, ³J_{H-H} = 7.9, ⁴J_{H-H} = 1.8 Hz, 1H, phen), 9.10 (dd, ³J_{H-H} = 4.4, ⁴J_{H-H} = 1.7 Hz, 1H, phen), 8.19 (d, ³J_{H-H} = 8.9 Hz, 2H, phenylNO₂), 7.84–7.71 (m, 6H, phenylNO₂, phenyl, phen), 7.60 (d, ³J_{H-H} = 8.9 Hz, 2H, phenyl), 7.47 (dd, ³J_{H-H} = 8.4, ⁴J_{H-H} = 1.7 Hz, 1H, phen), 7.34 (dd, ³J_{H-H} = 8.4, ⁴J_{H-H} = 4.3 Hz, 1H, phen) ppm. ES MS (*m/z*): [L + H]⁺ 417.1213 (calc. 418.1304). Anal. calc. for C₂₅H₁₅N₅O₂·CHCl₃ (%): C, 58.18; H, 3.00; N, 13.05. Found: C, 58.58; H, 3.03; N, 13.29.

Synthesis of Eu1 Complex. In a borosilicate glass round-bottom culture tube with a screw cap (Pyrex™, 1636/24MP), ligand L1 (100 mg, 349 μmol, 3 eq.), tetrabutylammonium hydroxide (271 mg, 698 μmol, 6 eq.), and Eu(OAc)₃·3H₂O (42 mg, 174 μmol, 1 eq.) were dissolved in acetone (16 mL). The solution was stirred at 50 °C overnight. The resulting mixture was extracted with dichloromethane (3 × 50 mL). Combined organic phases were dried over calcium(II) chloride and evaporated under a vacuum to give a yellow oily product; yield 70%. ¹H NMR (400 MHz, CDCl₃, 297 K) δ = 7.28 (s, 1H), 6.91 (d, ³J_{H-H} = 8.5 Hz, 1H, phenyl), 6.46 (d, ³J_{H-H} = 8.7 Hz, 1H, phenyl), 4.99 (s, 1H), 3.76–3.66 (m, 24H, NBu₄), 2.91 (s, 6H, NMe₂), 1.96–1.83 (m, 24H, NBu₄), 1.56 (q, ³J_{H-H} = 7.3 Hz, 24H, NBu₄), 1.05 (m, 36H, NBu₄) ppm. ES MS (*m/z*): [M-CO₂NCO₂]⁻ 769.0831 (calc. 769.0811). CHN analysis was obtained for potassium salt, which gives crystallizable powder suitable for analysis. Anal. calc. for C₅₁H₃₆EuK₃N₆O₁₂·(H₂O)₆ (%): C, 47.04; H, 3.72; N, 6.45. Found: C, 47.37; H, 4.02; N 6.18.

Synthesis of Eu2 Complex. The complex was synthesized according to a modified literature methodology [34]. In a round-bottom culture tube, Eu(TTA)₃·3H₂O (119 mg, 140 μmol, 1 eq.), L2 (50 mg, 140 μmol, 1 eq.) were dissolved in acetone (12 mL), the reaction mixture was stirred overnight at 50 °C. The precipitated yellow powder was centrifuged and washed three times with diethyl ether to eliminate the soluble ligand; yield 68%. ¹H NMR (400 MHz, DMSO, 297 K) δ = 18.70 (s, 2H, pyr), 10.54 (s, 2H, pyr), 10.02 (d, ³J_{H-H} = 8.5 Hz, 2H, phenyl), 9.40 (s, 2H, pyr), 7.51 (d, ³J_{H-H} = 8.7 Hz, 2H, phenyl), 6.89 (s, 3H, thioph), 6.11 (s, 3H, thioph), 5.47 (s, 3H, thioph), 3.98 (q, ³J_{H-H} = 7.2 Hz, 3H, NEt₂), 2.92 (s, 3H, CH), 1.55 (m, 6H, NEt₂) ppm. ES MS (*m/z*): [M + Na]⁺ 1199.0510 (calc.

1199.0572). Anal. calc. for $C_{43}H_{32}EuF_9N_8O_6S_3 \cdot CHCl_3 \cdot C_3H_6O$ (%): C, 43.11; H, 2.80; N 9.07; S 7.79. Found: C, 43.10; H, 3.04; N 8.41; S 7.24.

Synthesis of Eu3 Complex. In a round-bottom culture tube, $Eu(TTA)_3 \cdot 3H_2O$ (100 mg, 117 mmol, 1 eq.) and **L3** (50 mg, 117 mmol, 1 eq.) were dissolved into acetone (4 mL); the mixture was stirred overnight. The precipitated powder was centrifuged and washed three times with diethyl ether to eliminate the ligand, which was then recrystallized using gas-phase diffusion of diethyl ether into dichloromethane solution of the product. Light-yellow powder, quantitative yield: 57%. 1H NMR (400 MHz, acetone- d_6 , 297 K) δ = 14.37 (m, 1H, phen), 12.90 (m, 1H, phen), 9.36 (d, $^3J_{H-H}$ = 8.2 Hz, 1H, phen), 8.92 (d, $^3J_{H-H}$ = 8.0 Hz, 1H, phen), 8.85 (m, $^3J_{H-H}$ = 8.5 Hz, 3H, phen, phenyl), 8.67 (d, $^3J_{H-H}$ = 8.5 Hz, 2H, phenylNO₂), 8.62 (d, $^3J_{H-H}$ = 8.5 Hz, 2H, phenylNO₂), 8.36 (m, 3H, phenyl), 7.27 (m, 3H, thioph), 6.45 (m, 3H, thioph), 6.00 (m, 3H, thioph), 3.26 (m, 3H, CH) ppm. ES MS (m/z): $[M + Na]^+$ 1256.0008 (calc. 1255.9989). Anal. calc. for $C_{49}H_{27}EuF_9N_5O_8S_3 \cdot CH_2Cl_2$ (%): C, 46.01; H, 2.11; N, 5.42. Found: C, 46.03; H, 2.53; N, 5.05.

Synthesis of TPP-NHS ester. TPP-NHS ester was synthesized according to a slightly modified literature procedure [59]. *N,N'*-dicyclohexylcarbodiimide (357 mg, 1.73 mol, 2.4 eq.) and *N*-hydroxysuccinimide (100 mg, 0.86 mol, 1.2 eq.) were added to a solution of (2-Carboxyethyl)triphenylphosphonium bromide (**CE-TPP**) (300 mg, 0.72 mol, 1 eq.), in dry acetonitrile (10 mL), and the reaction mixture was stirred at room temperature for 12 h. The reaction mixture was cooled in the fridge and filtered to remove insoluble byproducts. The solvent was removed under reduced pressure to give the product as a light-beige solid, that was used without further purification. ^{31}P NMR (162 MHz, DMSO- d_6) δ 24.40. 1H NMR (400 MHz, DMSO) δ 7.98–7.89 (m, 3H), 7.89–7.74 (m, 12H), 4.09–3.92 (m, 2H), 3.15–3.01 (m, 2H).

Preparation of latex nanoparticles with embedded europium complexes. Latex nanoparticles (NPs) were synthesized according to [31]; however, the major feature of the obtained NPs was the surface primary amino groups originating from AEMA. A typical protocol for the preparation at 5 wt.% of solids is given: 5.8 mmol of MMA, 9.4 mmol of BMA, and 2.1 mmol of EGDMA were mixed, and a europium complex (8 mg) was then dissolved in monomers using an ultrasound bath for 5 min. CTAB (290 mg), AEMA (40 mg), and V-044 (30 mg) were added to a water/acetone mixture (95:5% *v/v*, respectively). The water solution was heated up to 70 °C and stirred in a 100 mL round-bottom flask for 3 min. The monomer solution was then added to a reaction system and polymerization was carried out for 25 min. The crude polymer dispersion was purified by exhaustive dialysis (Orange Scientific; molecular weight cutoff = 12–14 kDa) for 3 days to remove the residual monomers and the surfactant.

Ninhydrin assay. The concentration of primary amino groups was estimated by the colorimetric reaction with ninhydrin [60]. A NP suspension (1 mL) was added to 500 μ L ninhydrin reagent (1%, *w/v*) and heated in a boiling water bath for 15 min. The total volume was increased up to 5 mL and cooled to room temperature. UV absorbance was measured at a wavelength of 564 nm. AEMA was used to prepare the calibration curve.

Conjugation of latex NPs and triphenylphosphine. Conjugation was performed via surface amino groups of NPs and *N*-hydroxysuccinimidyl ester function of **TPP-NHS** as follows. 1 mL NPs (5.1 wt.%) was diluted in phosphate-buffered saline (PBS) with pH 7.4. TPP (6.68 mg, 0.024 mmol) was diluted in methanol and dropped in the PBS solution. The mixture was kept overnight at room temperature, and then, it was purified by exhaustive dialysis for 5 days to remove the residual molecules.

Particle size and ζ -Potential Measurements. The size, shape, and polydispersity index (PDI) of NPs were measured using dynamic light scattering (DLS; Malvern Nano ZS, Malvern, UK) and transmission electron microscopy (TEM; Jeol JEM-2100, Tokyo, Japan). TEM pictures were obtained in two cases: with and without negative staining by uranyl acetate (UrAc). The ζ -potential in the 10^{-3} M NaCl solution was also determined using The Malvern Zetasizer.

Inductively coupled plasma optical emission spectroscopy (ICPOES). The presence of Eu complexes and PS was determined using inductively coupled plasma optical emission

spectroscopy (ICPE-9000, Shimadzu). Europium nitrate and sodium hydrophosphate were used as references.

Photophysical experiments. The photophysical characteristics of the L1–L3 ligands and Eu1–Eu3 complexes were measured in distilled dichloromethane. Absorption UV-vis spectra were measured using a Shimadzu UV-1800 spectrometer (Shimadzu, Kyoto, Japan). Excitation and emission spectral data were recorded using a Fluorolog-3 (JY Horiba Inc., Kyoto, Japan) spectrofluorimeter. Quantum yields were calculated using a comparative method using LED 365 nm pumping and [Ru(bpy)₃](PF₆)₂ in water ($\Phi_r = 0.042$) as a standard [61]. The reference refraction indexes were: 1.33 (water), 1.42 (dichloromethane). The equation to calculate quantum yields [62]:

$$\Phi_S = \Phi_r \frac{\eta_S^2 \cdot A_r \cdot I_S}{\eta_r^2 \cdot A_S \cdot I_r} \quad (1)$$

where Φ_S —the quantum yield of the sample, Φ_r —the quantum yield of the reference, η —the refractive index of the solvent, A_s , A_r —the absorbance of the sample and the reference at the wavelength of excitation of emission, respectively, and I_s , I_r —the integrated area of emission band of the sample and the reference, respectively.

The value of the two-photon absorption cross-section was calculated by finding the value of the two-photon luminescence cross-section [63]:

$$\sigma_{\text{TPE}}^S = \sigma_{\text{TPE}}^r \cdot \left(\frac{n^S}{n^r}\right)^3 \cdot \frac{W^S/C^S/t^S}{W^r/C^r/t^r} \quad (2)$$

where σ_{TPE} is the two-photon luminescence cross-section, σ_{TPA} is the two-photon absorption cross-section ($\text{cm}^4 \cdot \text{s}$), $\sigma_{\text{TPE}} = \Phi \cdot \sigma_{\text{TPA}}$, where Φ is the luminescence quantum yield, W is the number of emitted photons, C is the molar concentration of the solution, n is the refractive index of the solvent, and t is the exposure time in seconds. As the cross-section for two-photon absorption and luminescence, the Goepfert–Mayer value, $10^{-50} \text{ cm}^4 \cdot \text{s} = 1 \text{ GM}$, was used. Fluorescein in aqueous solution at pH = 11 was used as the standard, its quantum yield was considered to be 91% [64], $\sigma_{\text{TPE}} = 43 \text{ GM}$ [63]. The concentration of the studied solutions was ca. 10^{-4} M . The concentration of latex particles in the dispersions under study was ca. $10^{-4}\%$ in the units of dry residue mass fraction.

Quantum yield and lifetime measurements for latex nanoparticles. The quantum yields of latex nanoparticles in a water dispersion were measured using a Quanta- ϕ integrating sphere with a modular spectrofluorimeter Fluorolog-3 (Horiba Jobin Yvon, Japan). A pulse laser TECH-263 Basic (wavelength, 263 nm; pulse width, 5 ns; and repetition frequency, 10–1000 Hz), an Ocean Optics monochromator (Monoscan-2000; interval of wavelengths, 1 nm), a FASTComTec (MCS6A1T4) multiple-event time digitizer, and a Hamamatsu (H10682-01) photon-counting head were used for lifetime measurements. Cyclic experiments for water dispersion of latex nanoparticles (~ 0.02 weight% of the dried residue) were performed in the temperature range of 20–40 °C using a temperature-controlled sample compartment qpod 2e (Quantum Northwest, Liberty Lake, WA, USA).

The lifetime vs. temperature calibration curves were obtained using the following protocol: (1) a sample of the probe aqueous dispersion was thermostated at 20 °C for 10 min (the optimized time that it made possible to stabilize the lifetime readings); (2) for the lifetime measurements, the resulting magnitude was the average of 5 times repetition; (3) the temperature was then increased by 5 °C, and the sample was thermostated for 10 min to make 5 independent measurements as above; (4) measurements were repeated in 5-degree increments until the temperature reached 40 °C.

The protocol for cyclic studies was similar to that used for building up the calibrations. The sensors' characteristics were calculated in accordance with the literature guidelines [5]. The calculations of temperature sensitivity (S_T), relative sensitivity (S_r), and reproducibility (R) are presented in ESI, Equations (S3)–(S5).

Experiments with CHO-K1 cell line. The Chinese hamster ovary CHO-K1 cells were cultured in DMEM/F12 (Biolog, St. Petersburg, Russia) medium supplemented with 10% FBS (Gibco, Carlsbad, CA, USA), 2 mM glutamine (Gibco, Carlsbad, CA, USA), and penicillin/streptomycin at a concentration of 100 U/mL (Thermo Fisher Scientific, Waltham, MA, USA). The cells were maintained in a humidified incubator at 37 °C with 5% CO₂ and passaged using trypsin-EDTA (Thermo Fisher Scientific, Waltham, MA, USA). For living-cell confocal microscopy, the cells (1×10^5 CHO-K1 cells in 1 mL DMEM) were seeded in glass-bottomed 35 mm dishes (Ibidi GmbH, Gräfelfing, Germany) and incubated for 24 h. Latex nanoparticles **NPs_Eu2** dispersed in water were dissolved in the growing media and added to the cells at a final concentration of 0.0195 wt.%. The dynamic of internalization was studied at different time points starting from 10 min. Before PLIM cell imaging, the cells were incubated with **NPs_Eu2** for 24 h in the glass-bottom dishes and then the medium was replaced with a fresh one.

MTT assay. The Chinese hamster ovary CHO-K1 cells (1×10^4 cells in 100 μ L of culture medium/well) were seeded in 96-well plates (TPP, TPP Techno Plastic Products AG, Trasadingen, Switzerland) and incubated overnight. The particles were added to the cells at concentrations of 0.0012–0.039 wt.% for 24 h. The solid content was calculated gravimetrically per 100 mL of water. Then, the cells were treated with the MTT reagent 3(4,5-dimethyl-2-thiazolyl)-2,5-diphenyl-2H-tetrazole bromide (Thermo Fisher Scientific, Waltham, MA, USA) at a concentration of 0.5 mg/mL. Following further incubation at 37 °C under 5% of CO₂ for 4 h, the formazan crystals were dissolved in DMSO, and the absorbance at 570 nm was measured using a SPECTROstar Nano microplate reader (BMG LABTECH, Ortenberg, Germany). The percentage of viable cells relative to the control was determined for each well as a ratio of the average absorbance value of the wells containing probes to that of the control wells. For each concentration of the particles, the experiment was repeated 12 times.

Vital staining of organelles. LysoTracker Deep Red (Thermo Fisher Scientific, Waltham, MA, USA) was used for the vital staining of acidified compartments, lysosomes, and late endosomes. BioTracker 405 Blue Mitochondria Dye (Merck KGaA, Darmstadt, Germany) was used for the vital staining of mitochondria. The CHO-K1 cells were incubated with **NPs_Eu2** and **NPs_Eu2_TPP** (0.0195 wt.%, 24 h). Then, the cells were rinsed with fresh media 3×1 mL, and incubated with a new portion of growing media for 15 min. LysoTracker Deep Red was added to the cells at a concentration of 50 nM and incubated 30 min prior to confocal imaging. BioTracker 405 was added to the cells at a concentration of 50 nM and incubated 15 min prior to confocal imaging.

Confocal microscopy and PLIM. Living CHO-K1 cells were imaged by using a confocal-inverted Nikon Eclipse Ti2 microscope (Nikon Corporation, Tokyo, Japan) with 60 \times oil immersion objective. The emission of europium was recorded in the range of 663–738 nm using single-photon excitation at 405 nm. In addition to luminescent microphotographs, differential interference contrast (DIC) images were also obtained. The images were processed and analyzed using ImageJ software (National Institutes of Health, Bethesda, MD, USA). The emission of the particles was excited with a 405 nm laser and recorded in the 570–620 nm (red channel) range. The fluorescence of LysoTracker Deep Red was excited at 638 nm and recorded at 663–738 nm. The fluorescence of BioTracker 405 Blue Mitochondria Dye was excited at 405 nm and recorded at 425–475 nm.

Phosphorescence lifetime imaging microscopy (PLIM) of CHO-K1 cells was carried out using the time-correlated single-photon counting (TCSPC). A DCS-120 module (Becker&Hickl GmbH, Berlin, Germany) integrated with the Nikon Eclipse Ti2 confocal device. A picosecond laser (405 nm) was used as an excitation source. The phosphorescence of the probe was recorded using a 575 longpass filter and 630/75 nm bandpass filter, and a pinhole of 0.5. PLIM images were obtained using the following settings: frame time of 42.87 s, pixel dwell time of 10.46 ms, points number of 1024, time per point of 10.00 μ s, time range of PLIM recording of 10.24 ms, total acquisition time of 87–131 s, and image size of 64 \times 64 pixels. Oil immersion 60 \times objective with zoom 7.11 provided a scan area of ca.

0.04 mm × 0.04 mm. Phosphorescence lifetime images were processed using SPCImage 8.1 software (Becker & Hickl GmbH, Berlin, Germany). All PLIM measurements were performed in a humidified Stage Top Incubator Tokai HIT (Fujinomiya, Japan) at 25, 30, or 40 °C and 5% CO₂. The phosphorescence decay curves were fitted in monoexponential mode. The average number of photons per curve was not less than 10,000 at binning 5–6.

4. Conclusions

The obtained novel europium complexes display desirable photophysical properties, namely, excitation with the bio-friendly visible (405 nm) and NIR (800 nm, TPE absorption) radiation and temperature dependence of emission characteristics (intensity and lifetime) in a physiologically relevant interval (20–40 °C). To avoid europium emission quenching in aqueous media, the complexes were successfully embedded into biocompatible latex nanoparticles (NPs_Eu1, NPs_Eu2, and NPs_Eu3) using nanoemulsion polymerization. Additionally, the surface of the NPs was modified with amino functions that provide a potential opportunity for their vectorization aimed at probe-targeted delivery. The photophysical properties of the europium chromophores remain nearly unchanged in the NPs, including lifetime sensitivity to temperature, with the highest one of 1.3%/K found for NPs_Eu2. For this probe, the investigation of cytotoxicity, internalization dynamics, and localization in CHO-K1 cells showed that it is possible to apply it safely in cell experiments. We also examined the NPs_Eu2 lifetime dependence on temperature under different conditions: in aqueous solution, in phosphate buffer, and in a mixture of the growth media (DMEM) and fetal bovine serum (FBS). The obtained data allow building up the calibration curve for temperature estimation in biological samples. PLIM experiments on the CHO-K1 cell line showed that this probe and obtained calibration curve can be used for the estimation of temperature in cells as well as for detection of the cell response to chemical shock, expressed as an increase in intracellular temperature. Unfortunately, vectorization of the probe surface with a phosphonium cation did not give its preferential localization in mitochondria that implies further studies to search for effective ways to deliver the probe to target cell compartments.

Supplementary Materials: The following supporting information can be downloaded at: <https://www.mdpi.com/article/10.3390/molecules27248813/s1>, Scheme S1: Scheme of L3 ligand synthesis; Figure S1: 1H NMR spectrum of ligand L3 in CDCl₃. S—residual solvent peak; Figure S2: 1H NMR spectrum of complex Eu1 in CDCl₃; Figure S3: 1H NMR spectrum of complex Eu2 in DMSO-d₆; Figure S4: 1H NMR spectrum of complex Eu3 in Acetone-d₆; Figure S5: Fragment of ESI⁺ spectrum of ligand L3; Figure S6: Fragment of ESI⁻ spectrum of complex Eu1; Figure S7: Fragment of ESI⁺ spectrum of complex Eu2; Figure S8: Fragment of ESI⁺ spectrum of complex Eu3; Figure S9: Excitation (solid lines) and emission (dashed lines) spectra of ligands in dichloromethane, 293K; Figure S10: Absorption spectra of Eu1–Eu3 complexes in dichloromethane, 293K; Figure S11: Excitation (solid lines) and emission (dashed lines) spectra of complex Eu1 in dichloromethane, 293K; Figure S12: Correlation between lifetimes of excited state and temperature for Eu3 in dichloromethane solution; Figure S13: Excitation (solid lines) and emission (dashed lines) spectra of complex Eu3 in dichloromethane, 293K; Figure S14: Correlation between lifetimes of excited state and temperature for Eu1 in dichloromethane solution; Figure S15: Excitation (solid lines) and emission (dashed lines) spectra of complex Eu1 in monomers taken with the same amount as for polymerization, 293K; Figure S16: Correlation between lifetimes of excited state and temperature for Eu2 in dichloromethane solution; Figure S17: Excitation (solid lines) and emission (dashed lines) spectra of complex Eu2 in monomers taken with the same amount as for polymerization, 293K; Figure S18: Excitation (solid lines) and emission (dashed lines) spectra of complex Eu3 in monomers taken with the same amount as for polymerization, 293K; Figure S19: Two-photon emission spectra of europium complexes in dichloromethane solution using 800 nm excitation wavelength, 293K; Equation (S1): temperature dependence of the excited-state lifetime; Figure S20: Main characteristics of NPs_Eu1. Dh—hydrodynamic diameter, PDI—polydispersity index, ζ-pot.—ζ-potential; Figure S21: Main characteristics of NPs_Eu2. Dh—hydrodynamic diameter, PDI—polydispersity index, ζ-pot.—ζ-potential; Figure S22: Main characteristics of NPs_Eu3. Dh—hydrodynamic diameter, PDI—polydispersity index, ζ-pot.—ζ-potential; Figure S23: Absorption spectra of latex nanoparticles in water dispersion, 293K;

Figure S24: Excitation (solid lines) and emission (dashed lines) spectra of nanoparticles with NPs_Eu1 in water dispersion, 293K; Figure S25: Excitation (solid lines) and emission (dashed lines) spectra of nanoparticles with NPs_Eu2 in water dispersion, 293K; Figure S26: Excitation (solid lines) and emission (dashed lines) spectra of nanoparticles with NPs_Eu3 in water dispersion, 293K; Equation (S2): Determination of the number of lanthanide complexes and triphenylphosphine per particle; Equation (S3): Temperature sensitivity ST; Equation (S4): Relative sensitivity Sr; Equation (S5): Reproducibility R; Figure S27: Correlation between lifetimes of excited state and temperature for NPs_Eu1 in water dispersion; Figure S28: Correlation between lifetimes of excited state and temperature for NPs_Eu2 in water dispersion; Figure S29: Dynamics of NPs_Eu2 (0.0195 wt%), accumulation by CHO-K1 cells during long-term incubation carried out in DMEM-F12 supplemented with 10% FBS. Confocal images: DIC image (top); green channel 500–550 nm (middle); red channel 570–620 nm (bottom). Scale bar 20 μm ; Figure S30: The NMR spectra of TPP-NHS ester (A) ^1H , (B) ^{31}P ; Figure S31: Main characteristics of NPs_Eu2_TPP. Dh—hydrodynamic diameter, PDI—polydispersity index, ζ -pot.— ζ -potential; Figure S32: Excitation (dashed line) and emission (solid line) spectra of nanoparticles with NPs_Eu2_TPP in water dispersion, 293K; Figure S33: (a) Temperature sensitivity of NPs_Eu2_TPP lifetime in different media: water, Dulbecco's buffer and model physiological medium (DMEM + 10%FBS). Interpolation of experimental data has been performed using Equation (1); (b) Cyclic lifetime measurements for NPs_Eu2 between 20 and 40 $^\circ\text{C}$ for NPs_Eu2 in water and DMEM + 10% FBS; Figure S34: (a) The dependence of emission intracellular intensity vs. incubation time of CHO-K1 with NPs_Eu2_TPP (b) Subcellular distribution of BioTracker 405 Blue Mitochondria Dye (blue color) and NPs_Eu2_TPP (red color) in CHO-K1 cells; (c) Subcellular distribution of LysoTracker Deep Red (blue color), and NPs_Eu2_TPP (red color) in CHO-K1 cells. Pearson's (P) and Manders' overlap coefficients (M1—fraction of tracker signal that overlaps conjugate signal, M2—fraction of conjugate signal that overlaps tracker signal) are presented as mean \pm standard deviation calculated for 50 cells. Scale bar 20 μm . Table S1. Temperature-dependent emission lifetimes of NPs_Eu2 and NPs_Eu2_TPP in media of various nature. Table S2. A comparison of Polymer NPs-Eu2 nanothermometer characteristics with those of published luminescent lifetime probes.

Author Contributions: Conceptualization, J.R.S. and S.P.T.; methodology, K.M.K., V.A.B., A.I.S. and E.E.G.; investigation K.M.K., V.A.B., A.I.S., E.E.G. and V.V.S.; data curation K.M.K., V.A.B., A.I.S., E.E.G., V.V.S. and A.F.K.; writing—original draft preparation, K.M.K., V.A.B., A.I.S., J.R.S. and S.P.T.; writing—review and editing, K.M.K., V.A.B., A.I.S., J.R.S. and S.P.T.; supervision, J.R.S. and S.P.T.; project administration, J.R.S. and S.P.T.; funding acquisition, S.P.T. All authors have read and agreed to the published version of the manuscript.

Funding: This research was funded by the Russian Science Foundation, grant number 19-13-00132-II.

Institutional Review Board Statement: Not applicable.

Informed Consent Statement: Not applicable.

Data Availability Statement: All data reported herein are accompanying the present article.

Acknowledgments: The experimental studies were carried out using equipment of the Research Park of St. Petersburg State University (Centers for Magnetic Resonance, for Optical and Laser Materials Research, for Chemical Analysis and Materials Research and for Molecular and Cell Technologies).

Conflicts of Interest: The authors declare no conflict of interest.

Sample Availability: Samples of the compounds Eu1–Eu3, NPs-Eu1–NPs_Eu3 are available from the authors.

References

1. Bai, T.; Gu, N. Micro/Nanoscale Thermometry for Cellular Thermal Sensing. *Small* **2016**, *12*, 4590–4610. [[CrossRef](#)] [[PubMed](#)]
2. Del Rosal, B.; Ximendes, E.; Rocha, U.; Jaque, D. In Vivo Luminescence Nanothermometry: From Materials to Applications. *Adv. Opt. Mater.* **2017**, *5*, 1600508. [[CrossRef](#)]
3. Nakano, M.; Nagai, T. Thermometers for Monitoring Cellular Temperature. *J. Photochem. Photobiol. C Photochem. Rev.* **2017**, *30*, 2–9. [[CrossRef](#)]
4. Dramićanin, M. Luminescence: The Basics, Methods, and Instrumentation. In *Luminescence Thermometry*; Elsevier: Amsterdam, The Netherlands, 2018; pp. 33–61.
5. Dramićanin, M.D. Trends in Luminescence Thermometry. *J. Appl. Phys.* **2020**, *128*, 040902. [[CrossRef](#)]

6. Ogle, M.M.; Smith McWilliams, A.D.; Jiang, B.; Martí, A.A. Latest Trends in Temperature Sensing by Molecular Probes. *ChemPhotoChem* **2020**, *4*, 255–270. [[CrossRef](#)]
7. Wang, X.; Wolfbeis, O.S.; Meier, R.J. Luminescent Probes and Sensors for Temperature. *Chem. Soc. Rev.* **2013**, *42*, 7834–7869. [[CrossRef](#)]
8. Qin, T.; Liu, B.; Zhu, K.; Luo, Z.; Huang, Y.; Pan, C.; Wang, L. Organic Fluorescent Thermometers: Highlights from 2013 to 2017. *TrAC Trends Anal. Chem.* **2018**, *102*, 259–271. [[CrossRef](#)]
9. Okabe, K.; Sakaguchi, R.; Shi, B.; Kiyonaka, S. Intracellular Thermometry with Fluorescent Sensors for Thermal Biology. *Pflug. Arch.* **2018**, *470*, 717–731. [[CrossRef](#)]
10. Li, R.; Xu, F.-F.; Gong, Z.-L.; Zhong, Y.-W. Thermo-Responsive Light-Emitting Metal Complexes and Related Materials. *Inorg. Chem. Front.* **2020**, *7*, 3258–3281. [[CrossRef](#)]
11. Zhang, K.Y.; Yu, Q.; Wei, H.; Liu, S.; Zhao, Q.; Huang, W. Long-Lived Emissive Probes for Time-Resolved Photoluminescence Bioimaging and Biosensing. *Chem. Rev.* **2018**, *118*, 1770–1839. [[CrossRef](#)]
12. Rocha, J.; Brites, C.D.S.; Carlos, L.D. Lanthanide Organic Framework Luminescent Thermometers. *Chem. Eur. J.* **2016**, *22*, 14782–14795. [[CrossRef](#)] [[PubMed](#)]
13. Abbas, M.T.; Khan, N.Z.; Mao, J.; Qiu, L.; Wei, X.; Chen, Y.; Khan, S.A. Lanthanide and Transition Metals Doped Materials for Non-Contact Optical Thermometry with Promising Approaches. *Mater. Today Chem.* **2022**, *24*, 100903. [[CrossRef](#)]
14. Wang, C.; Jin, Y.; Zhang, R.; Yao, Q.; Hu, Y. A Review and Outlook of Ratiometric Optical Thermometer Based on Thermally Coupled Levels and Non-Thermally Coupled Levels. *J. Alloys Compd.* **2022**, *894*, 162494. [[CrossRef](#)]
15. Ansari, A.A.; Parchur, A.K.; Nazeeruddin, M.K.; Tavakoli, M.M. Luminescent Lanthanide Nanocomposites in Thermometry: Chemistry of Dopant Ions and Host Matrices. *Coord. Chem. Rev.* **2021**, *444*, 214040. [[CrossRef](#)]
16. Dramićanin, M. Biomedical Applications of Luminescence Thermometry. In *Luminescence Thermometry*; Dramićanin, M., Ed.; Woodhead Publishing Series in Electronic and Optical Materials; Elsevier: Amsterdam, The Netherlands, 2018; pp. 235–250.
17. Li, H.; Zhao, Y.; Kolesnikov, I.; Xu, S.; Chen, L.; Bai, G. Multifunctional Rare Earth Ions-Doped Ba₂LaF₇ Nanocrystals for Simultaneous Temperature Sensing and Photothermal Therapy. *J. Alloys Compd.* **2023**, *931*, 167535. [[CrossRef](#)]
18. Savchuk, O.A.; Carvajal, J.J.; Haro-Gonzalez, P.; Aguiló, M.; Díaz, F. Luminescent Nanothermometry Using Short-Wavelength Infrared Light. *J. Alloys Compd.* **2018**, *746*, 710–719. [[CrossRef](#)]
19. Alkahtani, M.; Jiang, L.; Brick, R.; Hemmer, P.; Scully, M. Nanometer-Scale Luminescent Thermometry in Bovine Embryos. *Opt. Lett.* **2017**, *42*, 4812–4815. [[CrossRef](#)]
20. Brites, C.D.S.; Lima, P.P.; Silva, N.J.O.; Millán, A.; Amaral, V.S.; Palacio, F.; Carlos, L.D. Thermometry at the Nanoscale. *Nanoscale* **2012**, *4*, 4799–4829. [[CrossRef](#)]
21. Bustamante, N.; Ielasi, G.; Bedoya, M.; Orellana, G. Optimization of Temperature Sensing with Polymer-Embedded Luminescent Ru(II) Complexes. *Polymers* **2018**, *10*, 234. [[CrossRef](#)]
22. Santoro, S.; Sebastian, V.; Moro, A.J.; Portugal, C.A.M.; Lima, J.C.; Coelho, I.M.; Crespo, J.G.; Mallada, R. Development of Fluorescent Thermoresponsive Nanoparticles for Temperature Monitoring on Membrane Surfaces. *J. Colloid Interface Sci.* **2017**, *486*, 144–152. [[CrossRef](#)]
23. Fischer, L.H.; Stich, M.I.J.; Wolfbeis, O.S.; Tian, N.; Holder, E.; Schäferling, M. Red- and Green-Emitting Iridium(III) Complexes for a Dual Barometric and Temperature-Sensitive Paint. *Chem. Eur. J.* **2009**, *15*, 10857–10863. [[CrossRef](#)] [[PubMed](#)]
24. Fischer, L.H.; Karakus, C.; Meier, R.J.; Risch, N.; Wolfbeis, O.S.; Holder, E.; Schäferling, M. Referenced Dual Pressure- and Temperature-Sensitive Paint for Digital Color Camera Read Out. *Chem. Eur. J.* **2012**, *18*, 15706–15713. [[CrossRef](#)] [[PubMed](#)]
25. Karakus, C.; Fischer, L.H.; Schmeding, S.; Hummel, J.; Risch, N.; Schäferling, M.; Holder, E. Oxygen and Temperature Sensitivity of Blue to Green to Yellow Light-Emitting Pt(II) Complexes. *Dalton Trans.* **2012**, *41*, 9623–9632. [[CrossRef](#)] [[PubMed](#)]
26. Gállico, D.A.; Mazali, Í.O.; Sigoli, F.A. A Highly Sensitive Luminescent Ratiometric Thermometer Based on Europium(III) and Terbium(III) Benzoylacetate Complexes Chemically Bonded to Ethyldiphenylphosphine Oxide Functionalized Polydimethylsiloxane. *New J. Chem.* **2018**, *42*, 18541–18549. [[CrossRef](#)]
27. Werts, M.H.V. Making Sense of Lanthanide Luminescence. *Sci. Prog.* **2005**, *88*, 101–131. [[CrossRef](#)]
28. D'Aléo, A.; Picot, A.; Baldeck, P.L.; Andraud, C.; Maury, O. Design of Dipicolinic Acid Ligands for the Two-Photon Sensitized Luminescence of Europium Complexes with Optimized Cross-Sections. *Inorg. Chem.* **2008**, *47*, 10269–10279. [[CrossRef](#)]
29. Dramićanin, M. Lanthanide and Transition Metal Ion Doped Materials for Luminescence Temperature Sensing. In *Luminescence Thermometry*; Elsevier: Amsterdam, The Netherlands, 2018; pp. 113–157.
30. Cotton, S. Electronic and Magnetic Properties of the Lanthanides. In *Lanthanide and Actinide Chemistry*; John Wiley & Sons, Ltd.: Chichester, UK, 2006; pp. 61–87.
31. Shakirova, J.R.; Shevchenko, N.N.; Baigildin, V.A.; Chelushkin, P.S.; Khlebnikov, A.F.; Tomashenko, O.A.; Solomatina, A.I.; Starova, G.L.; Tunik, S.P. Eu-Based Phosphorescence Lifetime Polymer Nanothermometer: A Nanoemulsion Polymerization Approach to Eliminate Quenching of Eu Emission in Aqueous Media. *ACS Appl. Polym. Mater.* **2020**, *2*, 537–547. [[CrossRef](#)]
32. Galenko, E.E.; Novikov, M.S.; Shakirova, F.M.; Shakirova, J.R.; Korniyakov, I.V.; Bodunov, V.A.; Khlebnikov, A.F. Isoxazole Strategy for the Synthesis of 2,2'-Bipyridine Ligands: Symmetrical and Unsymmetrical 6,6'-Binicotinates, 2,2'-Bipyridine-5-Carboxylates, and Their Metal Complexes. *J. Org. Chem.* **2019**, *84*, 3524–3536. [[CrossRef](#)]
33. Karhunen, U.; Jaakkola, L.; Wang, Q.; Lamminmäki, U.; Soukka, T. Luminescence Switching by Hybridization-Directed Mixed Lanthanide Complex Formation. *Anal. Chem.* **2010**, *82*, 751–754. [[CrossRef](#)]

34. Lo, W.-S.; Kwok, W.-M.; Law, G.-L.; Yeung, C.-T.; Chan, C.T.-L.; Yeung, H.-L.; Kong, H.-K.; Chen, C.-H.; Murphy, M.B.; Wong, K.-L.; et al. Impressive Europium Red Emission Induced by Two-Photon Excitation for Biological Applications. *Inorg. Chem.* **2011**, *50*, 5309–5311. [[CrossRef](#)]
35. Englman, R.; Jortner, J. The Energy Gap Law for Radiationless Transitions in Large Molecules. *Mol. Phys.* **1970**, *18*, 145–164. [[CrossRef](#)]
36. Chelushkin, P.S.; Shakirova, J.R.; Kritchenkov, I.S.; Baigildin, V.A.; Tunik, S.P. Phosphorescent NIR Emitters for Biomedicine: Applications, Advances and Challenges. *Dalton Trans.* **2022**, *51*, 1257–1280. [[CrossRef](#)] [[PubMed](#)]
37. Baigildin, V.; Pankova, G.; Evseeva, T.; Lavrov, N.; Shirokova, I.; Vaganov, G.; Shevchenko, N. Methyl Methacrylate Particles with Amino Groups on the Surface: Colloid Stability and Sorption of Biologically Active Substances. *J. Dispers. Sci. Technol.* **2017**, *38*, 1570–1577. [[CrossRef](#)]
38. Su, X.; Wen, Y.; Yuan, W.; Xu, M.; Liu, Q.; Huang, C.; Li, F. Lifetime-Based Nanothermometry in Vivo with Ultra-Long-Lived Luminescence. *Chem. Commun.* **2020**, *56*, 10694–10697. [[CrossRef](#)] [[PubMed](#)]
39. Gao, H.; Kam, C.; Chou, T.Y.; Wu, M.-Y.; Zhao, X.; Chen, S. A Simple yet Effective AIE-Based Fluorescent Nano-Thermometer for Temperature Mapping in Living Cells Using Fluorescence Lifetime Imaging Microscopy. *Nanoscale Horiz.* **2020**, *5*, 488–494. [[CrossRef](#)]
40. Wang, Y.; Liang, S.; Mei, M.; Zhao, Q.; She, G.; Shi, W.; Mu, L. Sensitive and Stable Thermometer Based on the Long Fluorescence Lifetime of Au Nanoclusters for Mitochondria. *Anal. Chem.* **2021**, *93*, 15072–15079. [[CrossRef](#)]
41. Itoh, H.; Arai, S.; Sudhaharan, T.; Lee, S.-C.; Chang, Y.-T.; Ishiwata, S.; Suzuki, M.; Lane, E.B. Direct Organelle Thermometry with Fluorescence Lifetime Imaging Microscopy in Single Myotubes. *Chem. Commun.* **2016**, *52*, 4458–4461. [[CrossRef](#)]
42. Allison, S.W.; Gillies, G.T.; Rondinone, A.J.; Cates, M.R. Nanoscale Thermometry via the Fluorescence of YAG:Ce Phosphor Particles: Measurements from 7 to 77 °C. *Nanotechnology* **2003**, *14*, 859–863. [[CrossRef](#)]
43. Baleizão, C.; Nagl, S.; Borisov, S.M.; Schäferling, M.; Wolfbeis, O.S.; Berberan-Santos, M.N. An Optical Thermometer Based on the Delayed Fluorescence of C70. *Chem. Eur. J.* **2007**, *13*, 3643–3651. [[CrossRef](#)]
44. Peng, H.; Stich, M.I.J.; Yu, J.; Sun, L.; Fischer, L.H.; Wolfbeis, O.S. Luminescent Europium(III) Nanoparticles for Sensing and Imaging of Temperature in the Physiological Range. *Adv. Mater.* **2010**, *22*, 716–719. [[CrossRef](#)]
45. Shang, L.; Stockmar, F.; Azadfar, N.; Nienhaus, G.U. Intracellular Thermometry by Using Fluorescent Gold Nanoclusters. *Angew. Chem. Int. Ed.* **2013**, *52*, 11154–11157. [[CrossRef](#)] [[PubMed](#)]
46. Okabe, K.; Inada, N.; Gota, C.; Harada, Y.; Funatsu, T.; Uchiyama, S. Intracellular Temperature Mapping with a Fluorescent Polymeric Thermometer and Fluorescence Lifetime Imaging Microscopy. *Nat. Commun.* **2012**, *3*, 705. [[CrossRef](#)] [[PubMed](#)]
47. Sousa de Almeida, M.; Susnik, E.; Drasler, B.; Taladriz-Blanco, P.; Petri-Fink, A.; Rothen-Rutishauser, B. Understanding Nanoparticle Endocytosis to Improve Targeting Strategies in Nanomedicine. *Chem. Soc. Rev.* **2021**, *50*, 5397–5434. [[CrossRef](#)] [[PubMed](#)]
48. Hayashi, T.; Fukuda, N.; Uchiyama, S.; Inada, N. A Cell-Permeable Fluorescent Polymeric Thermometer for Intracellular Temperature Mapping in Mammalian Cell Lines. *PLoS ONE* **2015**, *10*, e0117677. [[CrossRef](#)]
49. Nakamura, T.; Matsuoka, I. Calorimetric Studies of Heat of Respiration of Mitochondria. *J. Biochem.* **1978**, *84*, 39–46. [[CrossRef](#)]
50. Gota, C.; Okabe, K.; Funatsu, T.; Harada, Y.; Uchiyama, S. Hydrophilic Fluorescent Nanogel Thermometer for Intracellular Thermometry. *J. Am. Chem. Soc.* **2009**, *131*, 2766–2767. [[CrossRef](#)]
51. Tsuji, T.; Ikado, K.; Koizumi, H.; Uchiyama, S.; Kajimoto, K. Difference in Intracellular Temperature Rise between Matured and Precursor Brown Adipocytes in Response to Uncoupler and β -Adrenergic Agonist Stimuli. *Sci. Rep.* **2017**, *7*, 12889. [[CrossRef](#)]
52. Kiyonaka, S.; Kajimoto, T.; Sakaguchi, R.; Shinmi, D.; Omatsu-Kanbe, M.; Matsuura, H.; Imamura, H.; Yoshizaki, T.; Hamachi, I.; Morii, T.; et al. Genetically Encoded Fluorescent Thermosensors Visualize Subcellular Thermoregulation in Living Cells. *Nat. Methods* **2013**, *10*, 1232–1238. [[CrossRef](#)]
53. Constant-Urban, C.; Charif, M.; Goffin, E.; van Heugen, J.-C.; Elmoualij, B.; Chiap, P.; Mouithys-Mickalad, A.; Serteyn, D.; Lebrun, P.; Pirotte, B.; et al. Triphenylphosphonium Salts of 1,2,4-Benzothiadiazine 1,1-Dioxides Related to Diazoxide Targeting Mitochondrial ATP-Sensitive Potassium Channels. *Bioorg. Med. Chem. Lett.* **2013**, *23*, 5878–5881. [[CrossRef](#)]
54. Peng, M.; Wang, X.-Q.; Zhang, Y.; Li, C.-X.; Zhang, M.; Cheng, H.; Zhang, X.-Z. Mitochondria-Targeting Thermosensitive Initiator with Enhanced Anticancer Efficiency. *ACS Appl. Bio Mater.* **2019**, *2*, 4656–4666. [[CrossRef](#)]
55. Chrétien, D.; Bénit, P.; Ha, H.-H.; Keipert, S.; El-Khoury, R.; Chang, Y.-T.; Jastroch, M.; Jacobs, H.T.; Rustin, P.; Rak, M. Mitochondria Are Physiologically Maintained at Close to 50 °C. *PLoS Biol.* **2018**, *16*, e2003992. [[CrossRef](#)] [[PubMed](#)]
56. Satapathy, R.; Padhy, H.; Wu, Y.-H.; Lin, H.-C. Synthesis and Characterization of Reversible Chemosensory Polymers: Modulation of Sensitivity through the Attachment of Novel Imidazole Pendants. *Chem. Eur. J.* **2012**, *18*, 16061–16072. [[CrossRef](#)] [[PubMed](#)]
57. Gomez Torres, S.; Pantenburg, I.; Meyer, G. Direct Oxidation of Europium Metal with Acetic Acid: Anhydrous Europium(III) Acetate, $\text{Eu}(\text{OAc})_3$, Its Sesqui-Hydrate, $\text{Eu}(\text{OAc})_3(\text{H}_2\text{O})_{1.5}$, and the “Hydrogendiacetate”, $[\text{Eu}(\text{H}(\text{OAc})_2)_3](\text{H}_2\text{O})$. *Z. Anorg. Allg. Chem.* **2006**, *632*, 1989–1994. [[CrossRef](#)]
58. De Silva, C.R.; Maeyer, J.R.; Wang, R.; Nichol, G.S.; Zheng, Z. Adducts of Europium β -Diketonates with Nitrogen p' -Disubstituted Bipyridine and Phenanthroline Ligands: Synthesis, Structural Characterization, and Luminescence Studies. *Inorg. Chim. Acta* **2007**, *360*, 3543–3552. [[CrossRef](#)]
59. Sodano, F.; Rolando, B.; Spyrakakis, F.; Failla, M.; Lazzarato, L.; Gazzano, E.; Riganti, C.; Fruttero, R.; Gasco, A.; Sortino, S. Tuning the Hydrophobicity of a Mitochondria-Targeted NO Photodonor. *ChemMedChem* **2018**, *13*, 1238–1245. [[CrossRef](#)] [[PubMed](#)]

60. Tauro, J.R.; Gemeinhart, R.A. Development of Amine-Containing Polymeric Particles. *J. Biomater. Sci. Polym. Ed.* **2005**, *16*, 1233–1244. [[CrossRef](#)]
61. Brouwer, A.M. Standards for Photoluminescence Quantum Yield Measurements in Solution (IUPAC Technical Report). *Pure Appl. Chem.* **2011**, *83*, 2213–2228. [[CrossRef](#)]
62. Resch-Genger, U.; Rurack, K. Determination of the Photoluminescence Quantum Yield of Dilute Dye Solutions (IUPAC Technical Report). *Pure Appl. Chem.* **2013**, *85*, 2005–2013. [[CrossRef](#)]
63. Melnikov, A.S.; Serdobintsev, P.Y.; Vedyaykin, A.D.; Khodorkovskii, M.A. Two-Photon Absorption Cross Section for Coumarins 102, 153 and 307. *J. Phys. Conf. Ser.* **2017**, *917*, 062029. [[CrossRef](#)]
64. Porrès, L.; Holland, A.; Pålsson, L.-O.; Monkman, A.P.; Kemp, C.; Beeby, A. Absolute Measurements of Photoluminescence Quantum Yields of Solutions Using an Integrating Sphere. *J. Fluoresc.* **2006**, *16*, 267–273. [[CrossRef](#)]